NJC

Accepted Manuscript

This is an *Accepted Manuscript*, which has been through the Royal Society of Chemistry peer review process and has been accepted for publication.

Accepted Manuscripts are published online shortly after acceptance, before technical editing, formatting and proof reading. Using this free service, authors can make their results available to the community, in citable form, before we publish the edited article. We will replace this *Accepted Manuscript* with the edited and formatted *Advance Article* as soon as it is available.

You can find more information about *Accepted Manuscripts* in the Information for Authors.

Please note that technical editing may introduce minor changes to the text and/or graphics, which may alter content. The journal's standard Terms & Conditions and the Ethical guidelines still apply. In no event shall the Royal Society of Chemistry be held responsible for any errors or omissions in this *Accepted Manuscript* or any consequences arising from the use of any information it contains.

ROYAL SOCIETY OF CHEMISTRY

www.rsc.org/njc

An Insight into Local environment of lanthanide ions in Sr_2SiO_4:Ln (Ln=Sm, Eu and Dy)

Santosh K. Gupta[1*], Sandeep Nigam[2], Ashok K. Yadav[3], Manoj Mohapatra[1], Shambhu N. Jha[3], Chiranjib Majumder[2], Dibyendu Bhattacharyya[3]

[1]Radiochemistry Division, [2]Chemistry Division, [3]Atomic and molecular physics Division

Bhabha Atomic Research Centre, Mumbai 400085, India

Abstract:

Sr_2SiO_4 is an important inorganic host for lanthanide doped white light emitting diodes. In order to probe the local structure and symmetry around lanthanide ions in Sr_2SiO_4, detailed experimental and theoretical investigation have been carried out. Samples prepared via sol-gel methods were thoroughly characterized using X-ray Diffraction (XRD), extended X-Ray Absorption Fine Structure (EXAFS) and photoluminescence (PL) spectroscopy. Local symmetry of SrO_9 and SrO_{10} polyhedra were determined using emission spectroscopy taking europium as the probe ion. Despite same oxidation state and comparable ionic radius, Sm^{3+}, Dy^{3+} and Eu^{3+}, behave differently in terms of their site occupation at Sr sites of the SrO_9 and SrO_{10} polyhedra. While Eu replaces Sr in both the polyhedra, Sm and Dy reside specifically in 9-coordnated Sr site only. Based on density functional theory (DFT) calculation it is established that for Dy and Sm, strong metal oxygen bonding leads to significant distortion and hence destabilization of MO_{10} polyhedra in the host.

Key words: Sr_2SiO_4; Site symmetry; Lanthanides; Photoluminescence; EXAFS

1.0 Introduction:

Strontium silicate is an important luminescence host as it has been extensively explored for white LEDs application. Park et. al has synthesized Eu^{2+} doped Sr_2SiO_4 yellow phosphor which was found to give white emission in combination with blue emitting GaN single crystal **[1]** and its efficiency was found to be better than commercially viable white phosphor. It was also reported that Ce^{3+} co-doping in Eu^{2+} doped Sr_2SiO_4 phosphor also leads to white emission **[2]**.

Large number of reports have been published recently in the literature pertaining to various technological applications of lanthanide ions doped Sr_2SiO_4 such as in solid state lighting **[3,4]**, as a thermochromic material [**5**], as a dosimeter [**6**], in long afterglow phosphor **[7]**, in IR detection **[8]** and in long lasting phosphorescence **[9]**.

Catti and Group **[10]** have discussed about the crystal structure of Sr_2SiO_4 and they have reported that its unit cell consists of two different types of strontium ion; nine coordinated Sr^{2+} (Sr-2) and 10-coordinated Sr^{2+} (Sr-1). They have also discussed about the

local symmetry of SrO_9 and SrO_{10} and confirmed that SrO_9 is relatively less symmetric than SrO_{10} which is having a hexagonal symmetry. In such systems where multiple doping sites are available (Sr-2 and Sr-1); spectroscopic information related to local site and its point symmetry is very crucial to optimize their optical performance for technological applications. Information about site occupancy can only be revealed from X-ray diffraction (XRD) at very high dopant ion concentration ($\geq$ 5.0 %) which may affect the efficiency of the luminescent material through concentration quenching. Thus actual site symmetry of the dopant in the cationic site can't be revealed from crystallographic data. Especially when these types of inorganic hosts are used to incorporate the lanthanide ions for luminescence application, it becomes extremely important to get the knowledge of site occupancy of particular Ln^{3+} ion. Further incorporation of Ln^{3+} ion at a particular site leads to change in the local surrounding environment in the doped host. Understanding these changes in the local environment is quite important for visualizing the overall changes in the host lattice. Further since luminescence properties are strongly dependent on the local structure around phosphor; it is of utmost importance to know the local symmetry around the lanthanide ions.

In an individual work we have extensively studied on luminescence properties of Sm^{3+}, Eu^{2+}, Eu^{3+} and Dy^{3+} **[11-14]**. Studying local site occupancy of lanthanide or any dopant ion in a system where multiple coordination or sites are available is very important for correlation between structural and various properties viz. optical, magnetic, catalytic etc. These properties are strongly influenced by local structure and site symmetry.

In the present work, we have given complete picture of lanthanide ion behavior in terms of their site occupancy in Sr_2SiO_4. We have carried out an exhaustive experimental and theoretical investigation to get in depth knowledge about the local symmetry of SrO_9 and SrO_{10} polyhedra of Sr_2SiO_4. Further, it is aimed to understand the factors responsible for substitution of Sr ions at different sites by three different rare earth ions Sm^{3+}, Dy^{3+} and Eu^{3+}. The choices of these three ions are guided by the fact that a combination of these three ions has potential to generate the white light. Time resolved fluorescence spectroscopy (TRFS) using emission spectra, emission kinetics and extended X-Ray Absorption Fine Structure *(EXAFS)* measurements have been used to establish the local environment around three lanthanide ions in the Sr_2SiO_4 host. To probe the type of defects formed on doping trivalent lanthanides ion in divalent Sr^{2+} site, positron annihilations spectroscopy were also carried out. These experimental results were further substantiated using density functional theory *(DFT)* calculations.

2.0 Experimental

2.1. Sample preparation:

All the chemicals employed for the sample preparation were of Analytical reagent (AR) grade and procured from Sigma Aldrich. Sr_2SiO_4 samples were prepared via a sol-gel route using tetraethyl orthosilicate (TEOS) for Si precursor and strontium nitrate for Sr precursor. High Purity oxides of Sm, Eu and Dy (SPEX Industries, INC., USA) are used for lanthanide ion doping. A detail of synthesis procedure is mentioned in our earlier work **[11-14]** For Eu^{2+} doped sample; Eu^{3+} doped Sr2SiO4 sample is subjected to heating at 600^{o}C for 6 h under reducing atmosphere (92 % Ar + 8% H_2) for conversion of Eu^{3+} to Eu^{2+}.

2.2. Instrumentation:

The phase purity of the prepared phosphor was confirmed by X-ray diffraction (XRD). The measurements were carried out on a STOE X-ray diffractometer equipped with scintillation counter and graphite monochromator. The diffraction patterns were obtained using monochromatic Cu-K_α radiation (λ= 1.5406Å) keeping the scan rate at 1sec. /step in the scattering angle range (2θ) of 10^{o} to 70^{o}. The $K_{\alpha 2}$ reflections were removed by a stripping procedure to obtain accurate lattice constants.

All the luminescence spectra were recorded using an Edinburgh FL920 instrument with variable frequency of 10-100 Hz equipped with a 150 W xenon lamp, M300 monochromator. Our systems are equipped with double monochromators in either or both excitation and emission arms. The use of double monochromators increases the linear dispersion and stray light suppression is improved over that achieved by single monochromators. It also consists of integrated control electronics CD920 and detector S900. Powder samples were dispersed in methanol for measurements. The data acquisition and analysis were done by F-900 software provided by Edinburgh Analytical Instruments, UK. A Xenon flash lamp with frequency range of 10–100 Hz was used as the excitation source. Emission spectrum for a particular sample was recorded with a lamp frequency of 100 Hz. Multiple Scans (at least five) were taken to minimize the fluctuations in peak intensity and maximize S/N ratio. Fluorescence lifetime measurements are based on well established Time-correlated single-photon counting (TCSPC) technique. EXAFS experiments were performed at Raja Ramanna Centre for Advanced Technology (RRCAT), Indore, India at dispersive beamline BL-8 in transmission mode using 2.5 GeV, 100 mA INDUS -2 synchrotron source. Other related information on instrumentation and sample preparation for EXAFS measurement is mentioned in our earlier report **[15-17]**.

3.0. Results and discussion

3.1. Powder X-ray Diffraction (PXRD): Phase Purity and Crystal structure

The purity and crystallinity of the as-prepared Sr_2SiO_4 and Sr_2SiO_4:Ln^{3+} (Ln = Eu, Dy, Sm) samples were characterized using powder X-ray diffraction (XRD). It can be seen that the from the XRD pattern in **Figure 1** that diffraction peaks of both Sr_2SiO_4 and Sr_2SiO_4:Ln^{3+} (Ln = Eu, Dy, Sm) samples were could be indexed to the orthorhombic phase of α'- Sr_2SiO_4 (JCPDS card No. 39-1256).

XRD data consisting of hkl values and interplanar spacing corresponding to α'- Sr_2SiO_4 was also evaluated **(ESI,† Table. T1)**. Incorporation of lanthanide ion has not change the XRD pattern which confirms that doping is proper and has not distorted the structure of strontium silicate. Since no impurity peaks were observed, it is feasible to suggest that both samples are a single phase of α'- Sr_2SiO_4. No obvious shifting of peaks or other impurity phases can be detected in the Ln^{3+}-doped samples, indicating that theLn^{3+} ions are efficiently dissolved in the Sr_2SiO_4 host lattice by replacing the Sr^{2+} because of the similar ionic radius and very small level of doping (0.5 mol %).

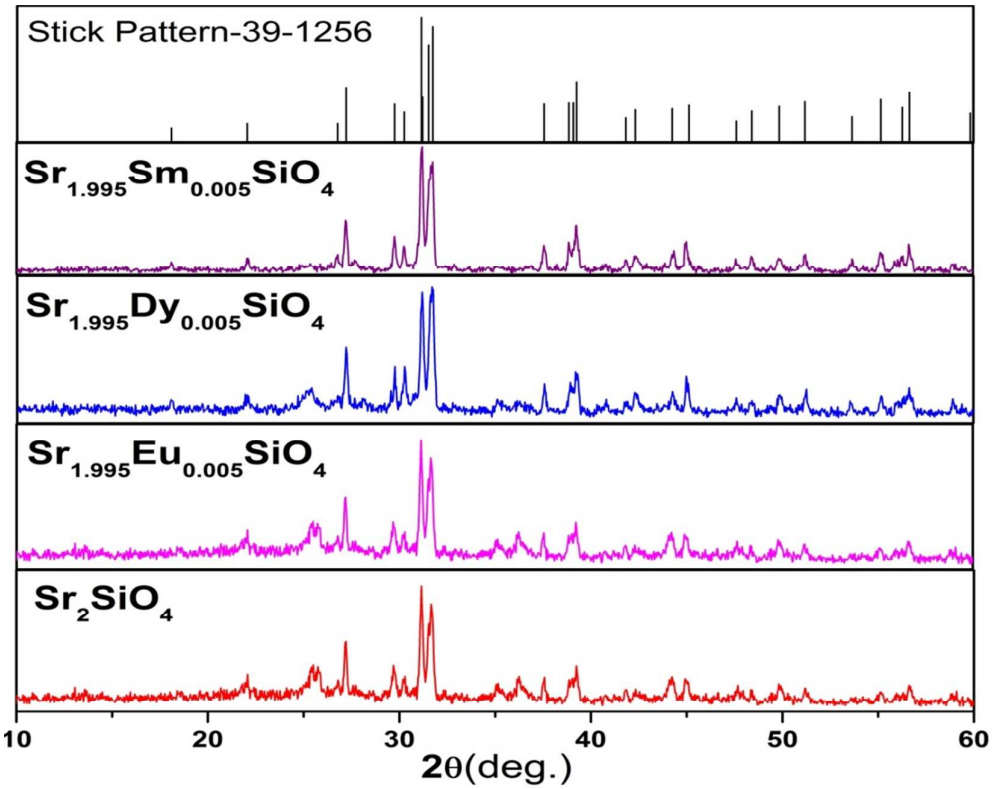

Figure 1: XRD pattern Sr_2SiO_4 and Sr_2SiO_4:Ln^{3+} (Ln = Eu, Dy, Sm)

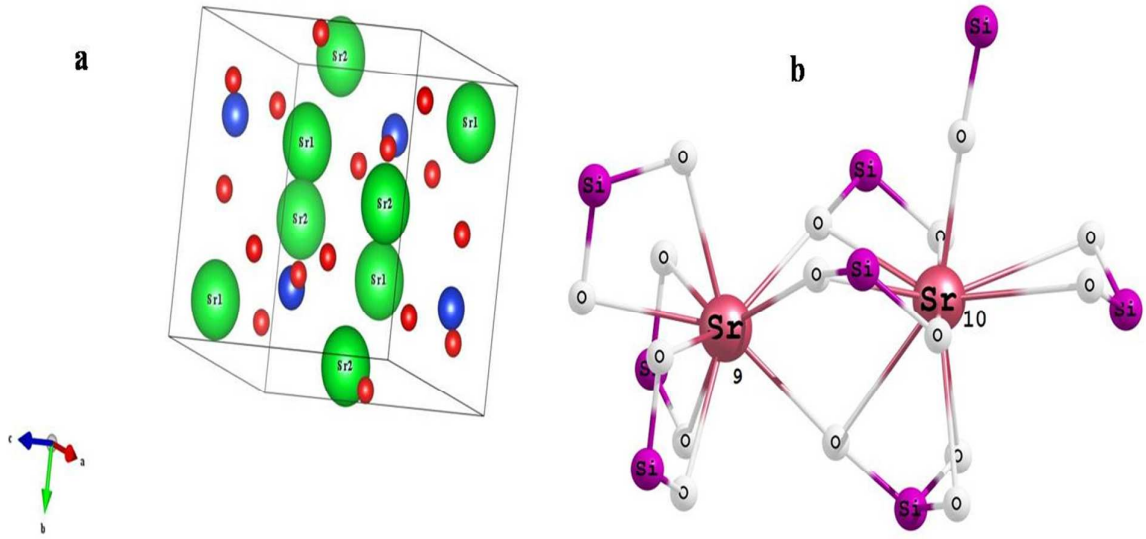

Figure 2: (a) Crystal structure of α'- Sr_2SiO_4 (b) Pictorial representation of 9-and 10-coordinated Sr^{2+} in strontium silicate

Figure 2 shows the crystal structure of α'- Sr_2SiO_4 and the coordination geometry of Sr^{2+} ion. Its structure is well described in literature and found close resemblance with similar non-closed packed K_2SiO_4 [18] structure. In one unit cell of α'- Sr_2SiO_4 there are 28 atoms 8 Sr, 4 Si and 16 O atoms. Out of 8 strontium atom 4 are Sr (1) and 4 are Sr (2) i.e. distribution ratio of SrO_9 and SrO_{10} is 50-50. A Si atom in SiO_4 tetrahedra forms a parallel chain. The Sr (1) sites are arranged in the form of linear chains (Si–O–Sr (1)–O–Sr (2)) whereas the Sr (2) sites displays zig-zag patterns of (Sr (1)–O–Sr (2)–O–Sr (1)) along the b-axis [19].

3.2. Photoluminescence Investigations:

3.2.1. $Sr_2SiO_4:Eu^{3+}$

The excitation spectrum of the 0.5 mol% sample with λ_{em} = 592 nm as mentioned in Figure 3 shows intense and broad band at ~243 nm (41152 cm^{-1}) and another relatively less intense band at ~ 296 nm (33784 cm^{-1}) both of which are assigned to the charge transfer band ; CTB-1 and CTB-2 respectively due to Sr (2) and Sr (1) polyhedra. In both cases the charge transfer is from $O^{2-} \rightarrow Eu^{3+}$ only; but oxygens are from different polyhedra i.e. SrO_9 and SrO_{10}. In one case it's Sr_9-O→Eu and in another case Sr_{10}-O→Eu CT. The peaks seen at 320, 360, 380 and 395 nm are due to the f-f transitions from the $^7F_0$ ground state to $^5H_3$, $^5L_9$, $^5G_3$ and $^5L_6$ (most intense) levels respectively. The existence of two charge transfer band further confirms the presence of two different types of Sr i.e. Sr (1) and Sr (2) α'- Sr_2SiO_4.

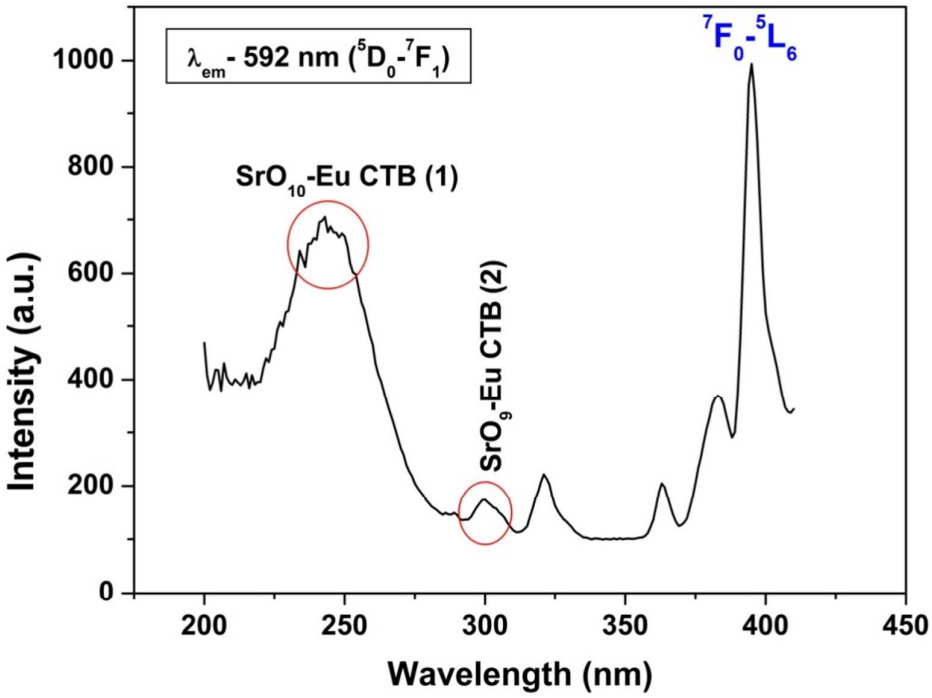

Figure 3: Excitation spectrum of Sr_2SiO_4: Eu^{3+} (0.5mol %)

To get an idea about the origin of CTB-1 at 243 nm and CTB-2 at 296 nm; emission spectra was recorded at both the wavelength and shown in **Figure 4**. The emission spectra recorded with 243 nm shows the typical features of europium ion at 575, 592, 615, 653 and 697 due to $^5D_0$ to ^7F_J transitions of Eu^{3+} where J= 0,1, 2, 3 & 4 respectively. Among all the transitions observed; the $^5D_0 \rightarrow {}^7F_1$ at 592 nm and $^5D_0 \rightarrow {}^7F_2$ at 615 nm are special one because of their peculiarity as symmetry sensitive transition and generally known as magnetic dipole transition (MDT) and hypersensitive electric dipole transition (EDT) respectively. Generally in a crystal site with inversion symmetry the EDT are strictly forbidden and the MDT is usually the most intense emission peak whereas in a site without inversion symmetry EDT is usually the strongest emission line, because transition $\Delta J = \pm 2$ are hypersensitive to small deviation from inversion symmetry. The more sensitive parameter for understanding symmetry is asymmetry ratio (I) which is described as ratio of integral intensities of EDT ($^5D_0 \rightarrow {}^7F_2$) to MDT ($^5D_0 \rightarrow {}^7F_1$). In spectra recorded at 243 nm excitation; there are two special characteristics: (i) intensity of $^5D_0 \rightarrow {}^7F_1$ at 592 nm and $^5D_0 \rightarrow {}^7F_2$ at 615 nm is comparable which is because of the fact that europium ion is distributed at site with inversion as well as non-inversion symmetry i.e. Sr (1) and Sr (2) and (ii) presence of $^5D_0$-$^7F_0$ line which is forbidden by both electric as well as magnetic dipole mechanism at high energy position (575 nm) than its usual position at around 580 nm. $^5D_0$-$^7F_0$ transition normally

appears when site symmetry is very low either C_n or Cnv [20]. This two observation confirms that Europium occupies both symmetric Sr(1) site as well as asymmetric Sr (2) site and 243 nm excite both the europium; Eu^{3+} sitting at Sr(1) and Sr (2) sites.

On the other hand emission spectrum recorded with 296 nm show entirely different characteristics. The first and the foremost observation is intensity of $^5D_0$-$^7F_0$ is more than all others and second one is absence of $^5D_0$-$^7F_1$ magnetic dipole transition. This shows that 296 nm is exciting europium ion sitting mostly at relatively asymmetric SrO_9 site.

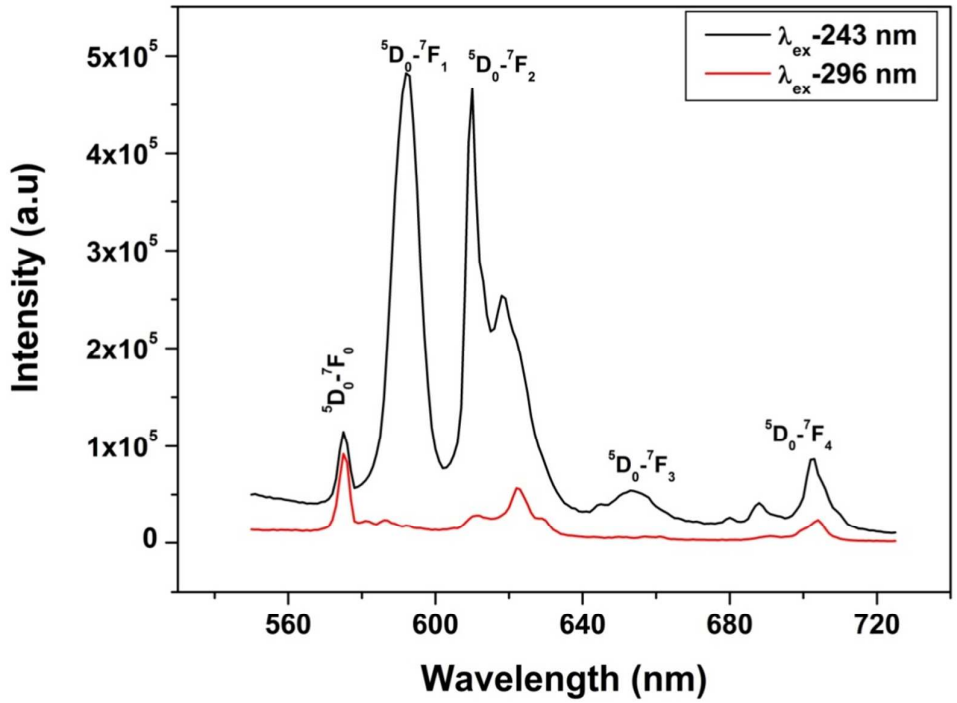

Figure 4: Emission spectrum of Sr_2SiO_4: Eu^{3+} with λ_{ex} = 243 nm and 296 nm.

It can be inferred from above discussion that 243 and 296 nm corresponding to charge transfer (O-Eu) from SrO_{10} and SrO_9 leads to entirely different emission characteristics. Looking from their respective emission spectrum it looks that 243 and 296 nm may be exciting different types of europium ion. To further substantiate the emission spectroscopy results photoluminescence decay measurements were carried. It can be seen from luminescence decay measurements using λ_{ex} of 243 nm **(ESI, † Fig. S1)**; biexponential behavior with lifetime value of 1.2 ms (Fast decaying, T_1) and 4.7 ms (slow decaying, T_2) was observed indicating the presence of europium ion at two different sites whereas monoexponential behavior is observed **(ESI, † Fig. S1)** on exciting with 296 nm with the lifetime of order 1.2 ms (only fast species, T_1). From all these discussion; we can say that

there are two types of europium ion; 1.2 ms and 4.7 ms (T_1 and T_2); 243 nm excite both of them where as 296 selectively excite 1.2 ms (T_1) species only.

Assuming a given phonon energy (same host for the lanthanide ions), a relatively longer PL decay time should be attributed to a more symmetric site, as the f-f transition becomes more forbidden, whereas a shorter decay time is often associated with an asymmetric site due to relaxation in the selection rules. Species T_1 (1.2 ms) arises because of Eu^{3+} ions occupying Sr (2) site without inversion symmetry whereas major species T_1 (4.7 ms) can be ascribed to Eu^{3+} ions occupying Sr (2) with inversion symmetry.

To elucidate the individual spectrum of species T_1 (1.2 ms) and T_2 (4.7 ms), time resolved emission spectroscopy was carried out using 243 nm as excitation wavelength. **Figure 5** shows the TRES individual spectra of T_1 and T_2 (Figure 6) which is arrived upon after proper slicing and mathematical calculation **(ESI, † Table. T2)**

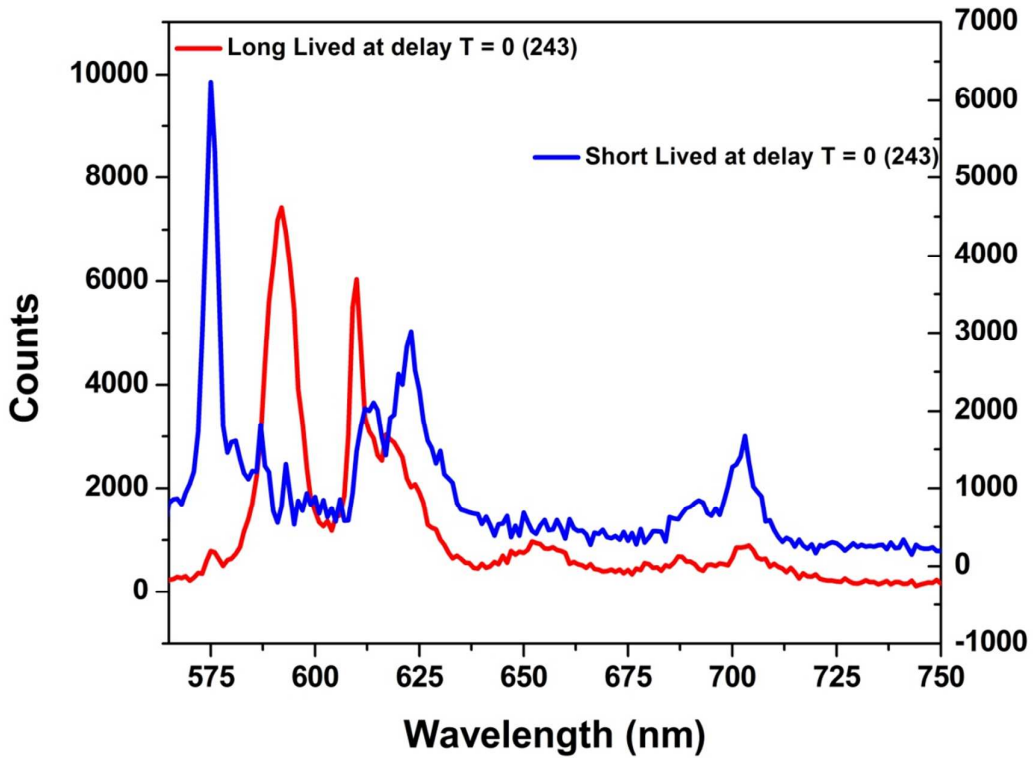

Figure 5: Emission spectra of the two RE ions species obtained after giving suitable delay times following TRES measurements (with 243 nm excitation).

It can be seen from the TRES spectra, for long lived species (T_2) intensity of MDT is more than EDT and $^5D_0$-$^7F_0$ is negligible seen whereas for short lived species $^5D_0$-$^7F_0$ is very intense, large splitting in spectral lines and MDT is absent or negligible present. From this

observation we can conclude that T_2 is present at symmetric 10-coordinated Sr (1) site whereas T_1 is present at relatively asymmetric 9-coordinated Sr (2) site.

3.2.2. Symmetry of 9- and 10-coordinated Strontium oxygen polyhedra in α'-Sr_2SiO_4

When the Eu^{3+} ion is inserted into any chemical/ligand environment (crystal field), the (2J + 1)-degenerate J-energy levels get splitted into the so-called Stark sub-levels by ligand field effect and the number of levels depending on the local site symmetry of the metal ion. The substitutions of Sr^{2+} with Eu^{3+} may results in significant lattice distortion due to size as well as charge difference. The peak at 575 nm in lower panel of **Figure 6** is due to $^5D_0 \rightarrow {}^7F_0$ transition of Eu^{3+} ion. Radiative transitions from $^5D_0$ to levels with $J = 0$ are both ED and MD forbidden, and only weak transitions from $^5D_0$ to these levels are observed due to CF induced J-mixing effect **[20]** . Moreover, the $^5D_0 \rightarrow {}^7F_0$ transition is only allowed in the following 10 site symmetries: C_s, C_1, C_2, C_3, C_4, C_6, C_{2V}, C_{3V}, C_{4V}, and C_{6V}, according to the ED selection rule **[21]**.

From stark splitting pattern shown for short lived species in **Figure 6**, one line for $^5D_0 \rightarrow {}^7F_0$ transition, three lines for $^5D_0 \rightarrow {}^7F_1$ magnetic dipole transition and four lines for $^5D_0 \rightarrow {}^7F_0$ electric dipole transition of Eu^{3+} were resolved whereas for long lived species shown in **Figure 7**,$^5D_0 \rightarrow {}^7F_0$ transition is absent but two lines for $J = 0 \rightarrow J = 1$ transition and three lines for $J = 0 \rightarrow J = 2$ transition of Eu^{3+} were resolved. According to the branching rules of various point groups **[20, 21, 22],** it infers that the actual site symmetry of T1 i the actual site symmetry of Eu^{3+}in 9-coordinated Sr-O polyhedra is C_{2V} whereas site symmetry of Eu^{3+}in 10-coordinated Sr-O polyhedra is C_{3V}.

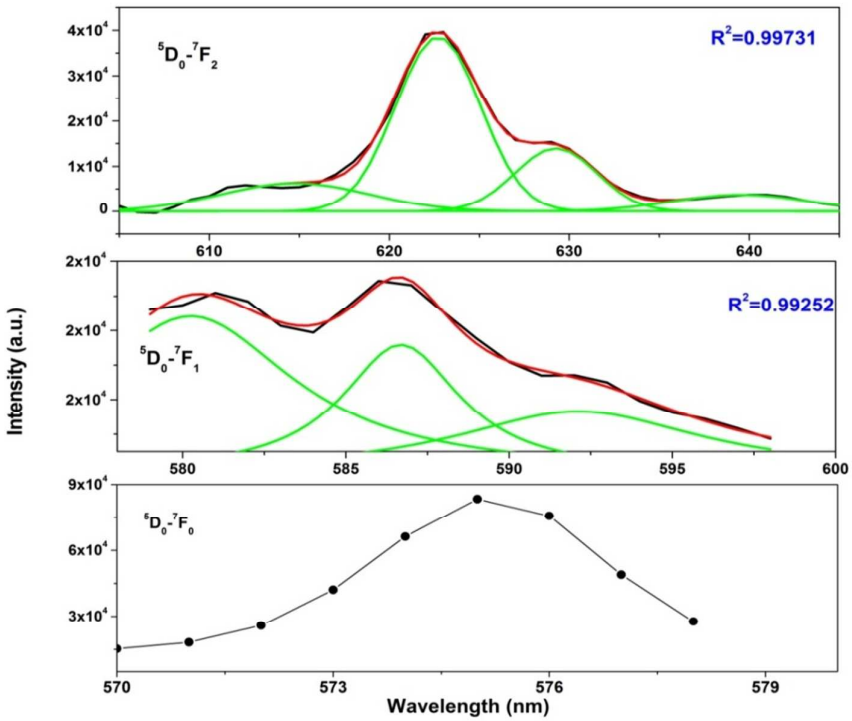

Figure 6: Gaussian fitted fluorescence spectra for short lived Eu^{3+} in sitting at 9-coordinated Sr^{2+}. Black line is the experimentally observed, red is Gaussian fitted and green indicates the deconvoluted components in each case.

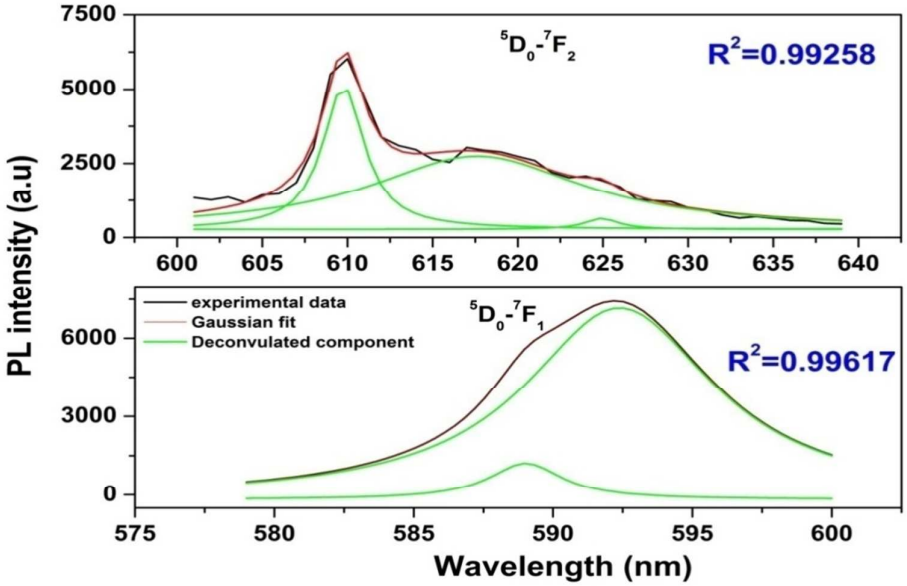

Figure 7: Gaussian fitted fluorescence spectra for selective region for long lived Eu^{3+} in sitting at 10-coordinated Sr^{2+}. Black line is the experimentally observed, red is Gaussian fitted and green indicates the deconvoluted components in each case.

3.2.3. $Sr_2SiO_4:Eu^{2+}$

Figure 8a shows the excitation spectra of $Sr_2SiO_4:Eu^{2+}$ at emission wavelength of 490 nm. The figure displays a broad band at around 340 nm which is assigned to $4f^7$ ($^8S_{7/2}$) – $4f^65d^1$ transition of the Eu^{2+} ions.

Since Eu^{2+} transitions involved 5d orbitals; effect due to crystal field can be seen in their emission spectra. **Figure 8b** shows the emission spectra of $Sr_2SiO_4:Eu^{2+}$ at excitation wavelength of 340 nm. The figure display two peaks at 490 nm (Eu_1) and 560 nm (Eu_2). This shows the stabilization of Eu^{2+} at two different sites.

Crystal field is related to radius using following equation:

$$D_q = \frac{1}{6} Ze^2 \frac{r^4}{R^5} \quad (1)$$

Where D_q is crystal field strength and R is radius.

It can be seen from the above mentioned equation; that crystal field strength is inversely proportion to ionic radii. Since in case of SrO_{10} and SrO_9; average Sr-O bond length is 2.85 and 2.69 Å respectively; crystal field strength at Sr-9 is more than that of Sr-10. Therefore, crystal field splitting of d-orbital will be more for Eu at Sr-9 site than at Sr-10 site. As a result energy difference between lowest electronic level in excited state and ground state is more in case of Sr-10. As a result more energy is required for de-excitation of Eu^{2+} at Sr-10 site than Sr-9 site; therefore emission is at lower wavelength. Therefore peak st 490 nm is because $Eu_{Sr(10)}$ and the one at 550 nm is due to $Eu_{Sr(9)}$.

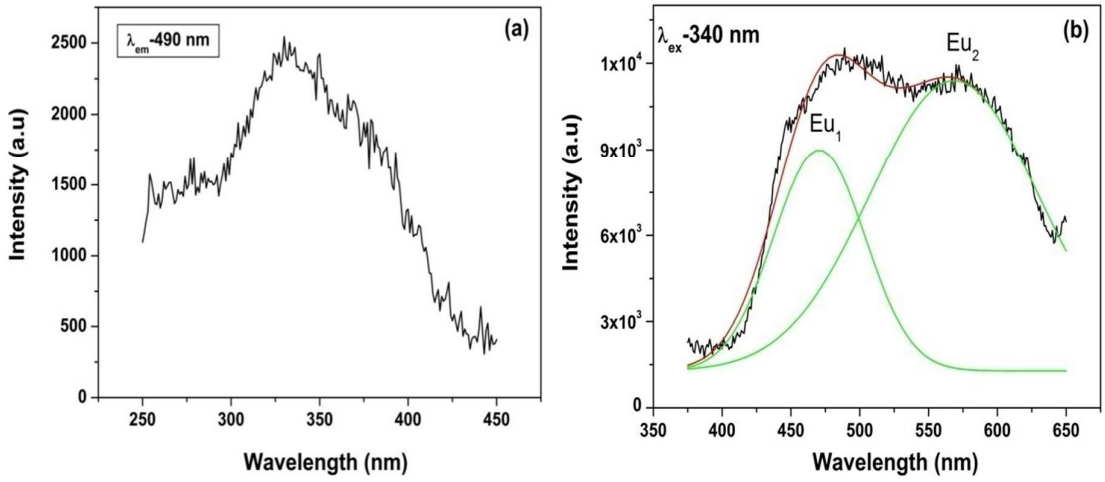

Figure 8: (a) Excitation spectrum (λ_{em}-490 nm) and (b) Emission spectrum (λ_{ex}-340 nm) $Sr_2SiO_4:Eu^{2+}$. Black line is the experimentally observed, red is Gaussian fitted and green indicates the deconvoluted components in each case.

The PL decay corresponding to emission at 490 and 560 nm (**ESI, † Fig. S2**) due to Eu^{2+} sitting at SrO_{10} site and SrO_9 site shows monoexponential behavior with the lifetime values of for 0.483 and 1.73 µs.

Based on phonon energy concept (same host for the lanthanide ions) , the longer lifetime should be attributed to the more symmetric site, as the electronic transition becomes more forbidden, corresponding to longer decay times. As discussed in the earlier section SrO_{10} is more symmetric than SrO_9.

Therefore 1.73 µs species arises because Eu^{2+} ions occupying symmetric 10-coordinate Sr (1) site whereas 0.483 µs species is due Eu^{2+} ion at relatively asymmetric 9-coordinated Sr (2) sites.

3.2.4. $Sr_2SiO_4:Dy^{3+}$

Figure 9a shows the photoluminescence excitation spectrum of $Sr_2SiO_4:Dy^{3+}$ monitoring emission at 576 nm. The excitation spectrum consisted of sharp lines at 326, 351, 366, 387, 427 and 450 nm which are attributed to f-f transition of Dy^{3+} ion. The origins of these peaks are labelled in excitation spectrum itself. The peak at 351 nm is the most intense which is ascribed to $^6H_{15/2} \rightarrow {}^6P_{7/2}$. **Figure 9b** shows the emission spectrum of $Sr_2SiO_4:Dy^{3+}$ at 351 nm excitation. The major peaks were located at 480 (blue), 574 (yellow) and 662 nm (red) which are due to $^4F_{9/2} \rightarrow {}^6H_{15/2}$ (blue), $^4F_{9/2} \rightarrow {}^6H_{13/2}$ (yellow) and $^4F_{9/2} \rightarrow {}^6H_{11/2}$ (red) transition respectively. The 480 nm peak (blue band) is due to magnetic dipole transition (MDT) and is generally insensitive to local site symmetry whereas 574 nm peak (yellow band) is hypersensitive electric dipole transition ($\Delta J = 2$, EDT) and is strongly affected by local environment/crystal field around of Dy^{3+} ion. The fact that 574 nm peak (EDT) is more intense than 480 nm peak (MDT) indicating that Dy^{3+} ion is located in site with low symmetry without any centre of inversion. Based on our discussion it can be confirmed that in Sr_2SiO_4; on doping majority of Dy^{3+} ion is situated in relatively asymmetric 9-coordinated Sr (2) sites.

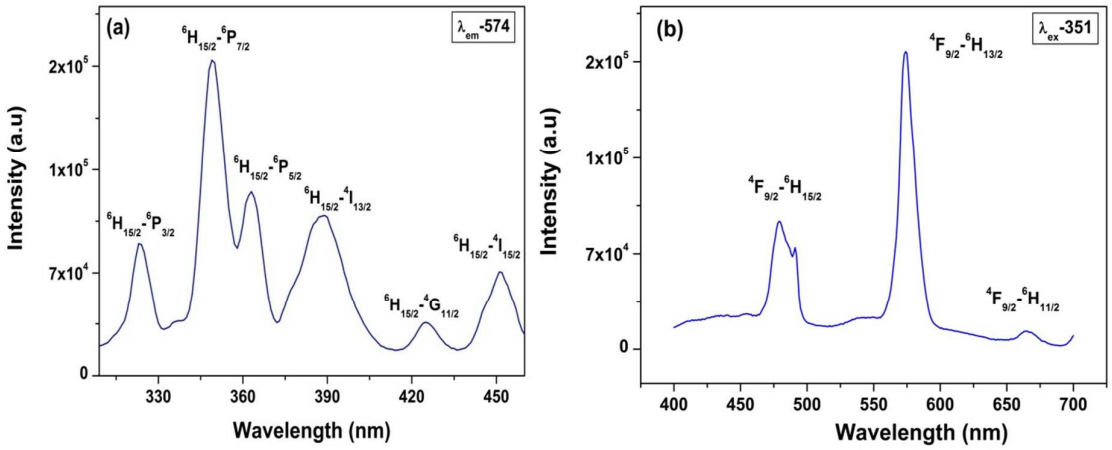

Figure 9: (a) Excitation and (b) Emission spectrum of the $Sr_2SiO_4:Dy^{3+}$

Photoluminescence (PL) life time decay measurement (**ESI, † Fig. S3)** of the $^4F_{9/2} \rightarrow {}^6H_{13/2}$ (yellow) transition for the $Sr_2SiO_4:Dy^{3+}$ system under excitation and emission wavelength of 351 and 574 nm respectively shows monoexponential behavior. So in Sr_2SiO_4; Dy^{3+} is homogenously distributed occupying relatively asymmetric 9-coordinated Sr site only.

3.2.5. $Sr_2SiO_4:Sm^{3+}$

Figure 10a shows the excitation spectrum of $Sr_2SiO_4:Sm^{3+}$ under the emission wavelength of 605 nm. Fine peaks in the wavelength range of 330-500 are displayed which are due to intra 4f transition of Sm^{3+} from $^6H_{5/2}$ ground state to higher energy levels of samarium ion. There are number of peaks at 346, 365, 379, 405, 417, 438, 462, 469, 473, and 485 nm which are ascribed to ($^6H_{5/2}$-$^6H_{13/2}$), ($^6H_{5/2}$-$^4D_{3/2}$), ($^6H_{5/2}$-$^6P_{7/2}$), ($^6H_{5/2}$-$^4F_{7/2}$), ($^6H_{5/2}$- $^6P_{5/2}$), ($^6H_{5/2}$-$^4G_{9/2}$), ($^6H_{5/2}$-$^4I_{9/2}$), ($^6H_{5/2}$-$^4I_{11/2}$), ($^6H_{5/2}$-$^4I_{13/2}$) and ($^6H_{5/2}$-$^4I_{15/2}$) transition respectively. The peak at 405 nm due to $^6H_{5/2}$-$^4F_{7/2}$ transition is the most intense peak. **Figure 10b** shows the emission spectrum recorded at 405 nm excitation. It displayed the typical emission profile of Sm^{3+} consisting of peaks at 562, 605, 641 and 711 nm due to $^4G_{5/2} \rightarrow {}^6H_{5/2}$, $^4G_{5/2} \rightarrow {}^6H_{7/2}$, $^4G_{5/2} \rightarrow {}^6H_{5/2}$ and $^4G_{5/2} \rightarrow {}^6H_{5/2}$ transitions respectively. Among the above mentioned transitions the one at 562 nm has magnetic dipole whereas as the other at 641 nm is having electric dipole character. The most intense peak at 605 nm is mixture of magnetic as well as electric dipole transition. The fact that electric dipole transition at 641 nm is more intense than magnetic dipole transition at 562 nm concludes that majority of Sm^{3+} is stabilized in asymmetric environment i.e. 9-coordinated Sr (2) site. Ionic radii analogy also supports the justification that Sm^{3+} preferentially occupies Sr (2) site because size difference between 9-coordinared Sm^{3+} and 9-coordinated Sr^{2+} are less than between 10-coordinated Sm^{3+} and Sr^{2+}

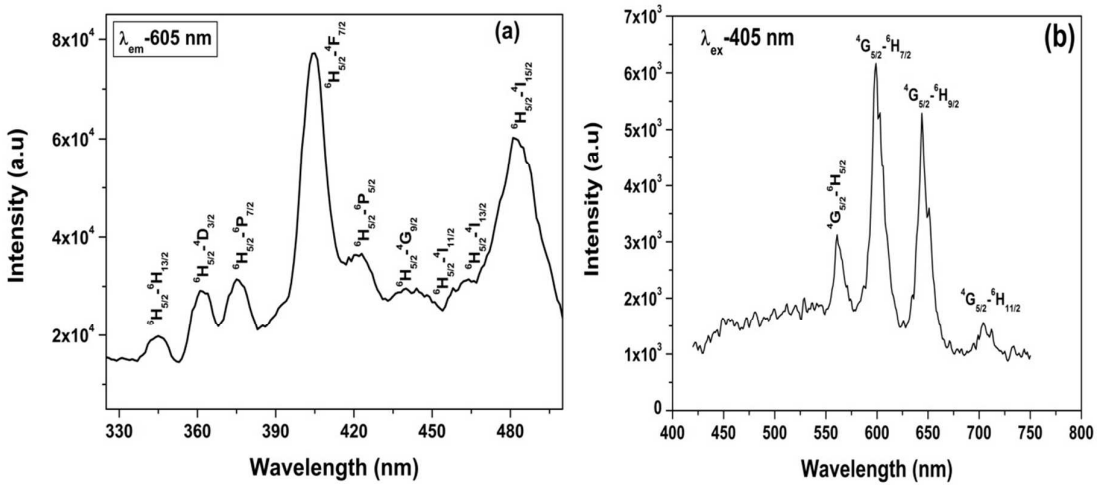

Figure 10: (a) Excitation and (b) Emission spectrum of the $Sr_2SiO_4:Sm^{3+}$

To get clearer picture about local site around Sm^{3+} ion in strontium silicate host; lifetime measurements at excitation and emission wavelength of 405 and 605 nm were carried out. PL decay curve for $Sr_2SiO_4:Sm^{3+}$ (**ESI, † Fig. S4)** shows monoexponential profile with lifetime value of 2.3 ms indicating homogenous distribution of Sm^{3+} ion in Sr_2SiO_4. Based on fluorescence lifetime and emission spectroscopy results, it can be inferred that Sm^{3+} mainly occupies 9-coordinated Sr (2) site in Sr_2SiO_4.

3.4. X-ray Absorption spectroscopy

3.4.1. Extended X-Ray Absorption Fine Structure (EXAFS): Normalized and Fourier Transform

Figure 11 show the normalized EXAFS spectra ($\mu(E)$ versus E) for blank Sr_2SiO_4 along with Eu, Dy and Sm doped Sr_2SiO_4.

In order to take care of the oscillations in the absorption spectra $\mu(E)$ has been converted to absorption function $\chi(E)$ defined as follows **[23]**:

$$\chi(E) = \frac{\mu(E) - \mu_0(E)}{\Delta\mu_0(E_0)} \qquad (1)$$

Where E_0 absorption edge energy, $\mu_0(E_0)$ is the bare atom background and $\Delta\mu_0(E_0)$ is the step in $\mu(E)$ value at the absorption edge. The energy dependent absorption coefficient

$\chi(E)$ has been converted to the wave number dependent absorption coefficient $\chi(k)$ using relation,

$$K = \sqrt{\frac{2m(E-E_0)}{\hbar^2}} \qquad (2)$$

Where m is the mass of electron and h is Planck's constant. $\chi(k)$ is weighted by k^2 to amplify the oscillation at high k and the $\chi(k)k^2$ functions are Fourier transformed in R space to generate the $\chi(R)$ versus R spectra in terms of the real distances from the center of the absorbing atom. The set of EXAFS data analysis available in within IFEFFIT software package have been used for EXAFS data analysis **[24]**. This includes background reduction and Fourier transform to derive the $\chi(R)$ versus R spectra from the absorption spectra (using ATHENA software), generation of the theoretical EXAFS spectra starting from an assumed crystallographic structure and finally fitting of experimental data with the theoretical spectra using ARTEMIS software.

The $\chi(R)$ versus R spectra have been generated for all the samples from the $\mu(E)$ versus E spectra following the methodology described above and the best fit $\chi(R)$ versus R spectra of the samples have been shown in Fig. 16.The structural parameters (atomic coordination and lattice parameters) of Sr_2SiO_4 used for simulation of theoretical EXAFS spectra of the samples have been obtained from reported values in the literature **[10, 13]**. There are two crystallographic sites of Strontium in structure in which one is 10 coordinated and another is 9 coordinated. The scattering paths are generated using each Sr atom as central atom and have been used in the fitting of the experimental data with 50% weightage given to each crystallographic site. The bond distances, co-ordination numbers (including scattering amplitudes) and disorder (Debye-Waller) factors (σ^2), which give the mean square fluctuations in the distances, have been used as fitting parameters and summarized in tabular form **(ESI,† Table. T3)**

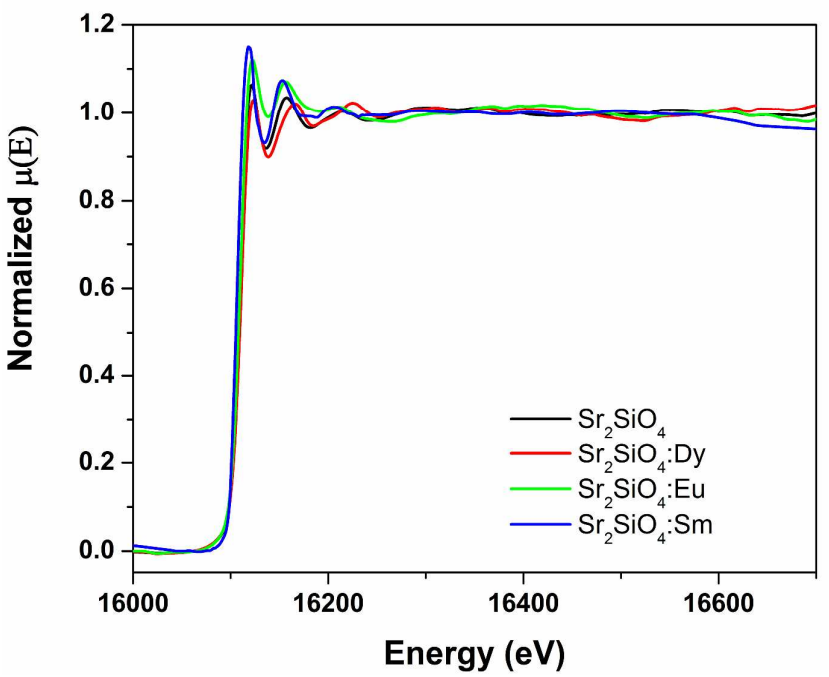

Figure 11: Normalized EXAFS spectra of blank Sr_2SiO_4 along with Eu, Dy and Sm doped Sr_2SiO_4

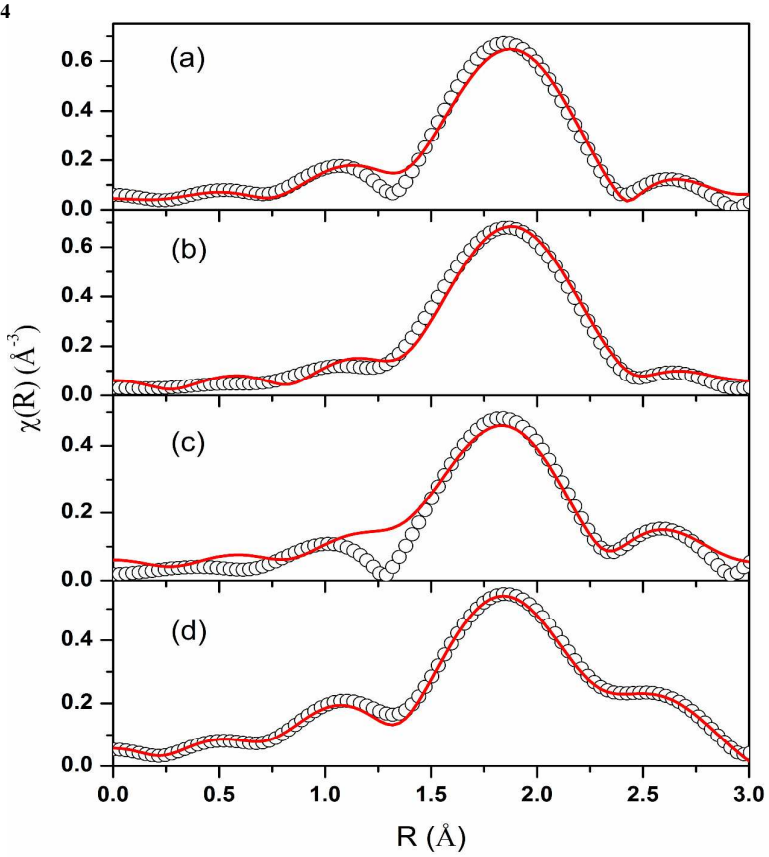

Figure 12: Fourier transformed EXAFS spectra at Sr K-edge (Scatter points) and theoretical fit (Solid line) for (a) Sr_2SiO_4 (b) Dy doped Sr_2SiO_4 (c) Eu doped Sr_2SiO_4 and (d) Sm doped Sr_2SiO_4

3.4.2. Eu Doped Sr_2SiO_4:

From EXAFS data (**ESI,† Table. T3)** it was seen that on average bond lengths remain unchanged on Eu doping, which can be explained as the ionic radii of 10-coordinated Eu^{2+} (1.35 Å) and 9-coordinated Eu^{2+} (1.30 Å) are close to 10 coordinated Sr^{2+} (1.36 Å) and 9-coordinated Sr^{2+} (1.31 Å) respectively **[25]**. There is an increase in σ^2values for both Sr(1)-O and Sr(2)-O bonds, which manifests increase in disorder at both the Sr sites and thus corroborates the earlier results that Eu incorporates in both 10 and 9 coordination sites . However, is has been observed that the change in σ^2 value is higher for 9-coordinated Sr site than for 10-coordinated Sr site which may be due to higher Eu incorporation in 9-coordinated site than in 10-coordination sites. Nguyen *et al.* **[26]** has also reported preferentially higher Eu substitution in 9-coordinated Sr sites on the basis of enhanced intensity of the yellow luminescence.

3.4.3. Dy Doped Sr_2SiO_4:

The average Sr(2)-O bond length is found to decrease in Dy doped samples compared to the undoped samples (**ESI,† Table. T3)**, however there is no change appeared in Sr(1)-O average bond length. This decrease in Sr(2)-O bond length can be due the smaller ionic size of Dy^{3+} (1.083 Å for 9 coordination) than Sr^{2+} ion (1.31 Å for 9 coordination) **[25]**. It may be possible that Dy ions only occupy Sr (2) site and not Sr (1) site since 10-coordinated Dy geometry does not exist **[25]**, however, EXAFS measurements at Dy edge is required to ascertain that.

3.4.4. Sm Doped Sr_2SiO_4:

The average Sr(1)-O and Sr(2)-O bond lengths are found to decrease (**ESI,† Table. T3)** in Sm doped samples compared to the undoped samples. It is also observed that σ^2 which is mean square displacement parameter is increased for Sr(2)-O bonds indicating that 9 coordinated Sr sites are replaced by Sm ions.

3.5. Computational Results:

In order to rationalize the experimental results and to get insight about the local structure, theoretical calculations were carried out on Sr_2SiO_4 (undoped and doped with Eu/Sm/Dy atom). All calculations were carried out using the spin-polarized DFT with a plane wave basis set, implemented in the Vienna Ab-initio Simulation Package (VASP). The electron–ion interactions were described by the projector augmented wave (PAW) method. The spin polarized generalized gradient approximation using the Perdew–Burke–Ernzerhof (PBE) functional has been used to calculate the exchange-correlation energy. The cut off

energy for the plane wave basis set was fixed at 400 eV. The geometry optimization was performed by ionic relaxation, using a conjugate gradient minimization. The geometries are considered to be converged when the force on each ion becomes 0.01eV/ Å or less. The total energy convergence was tested with respect to the plane-wave basis set size and simulation cell size, and the total energy was found to be accurate to within 1 meV. Three-dimensional periodic boundary conditions were applied to approximate a bulk solid (i.e. orthorhombic phase of Sr_2SiO_4). Conventional cubic unit ($\alpha = \beta = \gamma = 90^o$) cell containing 28 atoms (8 Sr, 4 Si, 16 O) were used for calculations. Structural optimization was performed with respect to atomic coordinates and unit-cell parameters. A Monkhorst-Pack k-point grid of 3 x 3 x 3 was employed to map the first Brillouin zone. For the orthorhombic unit cell, the lattice parameters were found to be a= 5.673 Å b= 7.073 Å and c= 9.766 Å. These values are excellent in comparison to the experimental lattice constants (a= 5.682 Å b= 7.091 Å and c= 9.772 Å). In case of doped Sr_2SiO_4, out of 8 Sr atoms of unit cell, one atom was replaced with Eu/Sm/Dy atom. As mentioned previously, two types of Sr atom (9-coordinated and 10-coordinated) are presented in Sr_2SiO_4, therefore both 9 and 10-coordinated sites were considered for replacement, and optimizations were carried out without any symmetry constraint. The energetics of the doped structures is tabulated (**ESI,† Table. T4)**

Energetically it is clear that 9-coordinated site is more favourable than its 10-coordinated counterpart (**ESI, † Table. T4).** . However, it is worth to notice that difference in stability forEu^{3+} doping between the 9 and 10 coordination sites is only 0.03 eV (of the order of room temperature energy). In contrast, for Dy and Sm doping, the difference in stability between two sites is much higher (~0.6-0.7 eV). These results are in excellent agreement with those obtained by experimental methods, where both Dy and Sm were found to occupy only 9 coordination sites and the presence of Eu at both 9 and 10 coordinated sites was reported. Thus it can be inferred that destabilization of 10 coordination occupancy by strong metal oxygen bond for Dy and Sm, is the cause for such an observation.

In order to further rationalize the results, we focused our attention on the geometrical aspects of the SrO_9 and SrO_{10}polyhedra of Sr_2SiO_4 compound. In SrO_9 polyhedra, the average Sr-O bond length is found to be 2.68 Å, (Shortest bond: 2.50 Å, largest bond: 3.04 Å), and for SrO_{10} polyhedra, the average Sr-O bond length is found to be 2.84 Å, (Shortest bond: 2.38 Å, largest bond: 3.04 Å) (**ESI, † Fig. S5 and S6)**. The theoretically calculated value of average Sr-O bond length of SrO_9 and SrO_{10} polyhedra are in agreement with the experimental values of 2.698 Å and 2.852 Å **[13]**. Further symmetry observed of these two polyhedral (C_{2v} for

SrO_9 and C_{3v} for SrO_{10}) are shown in **Figure 13** and tabulated (**ESI, † Table. T5**). It can be seen from the table that SrO_9 has lower symmetry of C_{2V} than that of SrO_{10} which is having C_{3v} symmetry. The relatively higher symmetry of SrO_{10} polyhedra is in line with the experimental result presented in section 3.2.2, as well as previous reports **[10]**.

Importantly, SrO_{10} polyhedra has a short Sr-O bond with 2.38 Å, which is not present in the SrO_9 polyhedra. Further, we noticed that substitution of Eu at Sr, does not distort the original SrO_9 and SrO_{10} polyhedra (**ESI, † Fig. S7**), but inclusion of Dy and Sm leads to distortion of polyhedra to greater extent (**ESI, † Fig. S8 and S9**). In particular, substitution of Sr in SrO_{10} polyhedra by Dy and Sm leads to substantial changes by reducing shortest metal oxygen bond from 2.38Å values of original SrO_{10}polyhedra to 2.18/2.29Å respectively. Simultaneously, few other M-O bonds were also reduced. Contraction of these M-O bond leads to elongation of some other M-O bond (from 2.8-3.0 Å value of original SrO_{10}polyhedra to 2.9-3.5/2.9-3.2 Å for DyO_{10}/SmO_{10}. This observed distortion is in line with energetics values presented in table-4, where the stability difference for Dy and Sm substitution at 9 and 10-coordination site was found to be quite large ~0.6-0.7 eV. It is worth to mention despite comparable ionic radii of these three cation, Sm^{3+}(1.13 Å) , Eu^{3+} (1.12 Å) , Dy^{3+} (1.09 Å) with Sr^{2+} ion, but the metal oxygen bond strength for the M-O dimer (M= Eu, Dy, Sm) is quite different for the three. The values in eV/atom follow the following trend: [Sr-O (2.66) <Eu-O (2.95) <Sm-O (3.58) <Dy-O (3.84) **[27]**].

Therefore, on the basis of these results it is inferred that Dy and Sm form much stronger bond with oxygen in comparison to Sr and Eu (Sr and Eu have comparable values). Stability of Dy-O/Sm-O bond leads to formation of few strong metal-oxygen bonds in DyO_{10}/SmO_{10}, by losing other metal-oxygen bond of polyhedral. Thus, relatively enhanced stability of Dy-O/Sm-O bond leads to contraction of few metal-oxygen bonds. As a consequence, remaining metal-oxygen bonds become weaker or elongated. This asymmetrical contraction/elongation phenomenon in the DyO_{10}/SmO_{10}polyhedron leads to significant distortion with respect to original SrO_{10}polyhedra. These results very well explains that in experiments, Eu-atom could substitute the Sr at both 9 and 10 coordinated site however; Dy and Sm could not substitute the Sr at 10 coordinated sites.

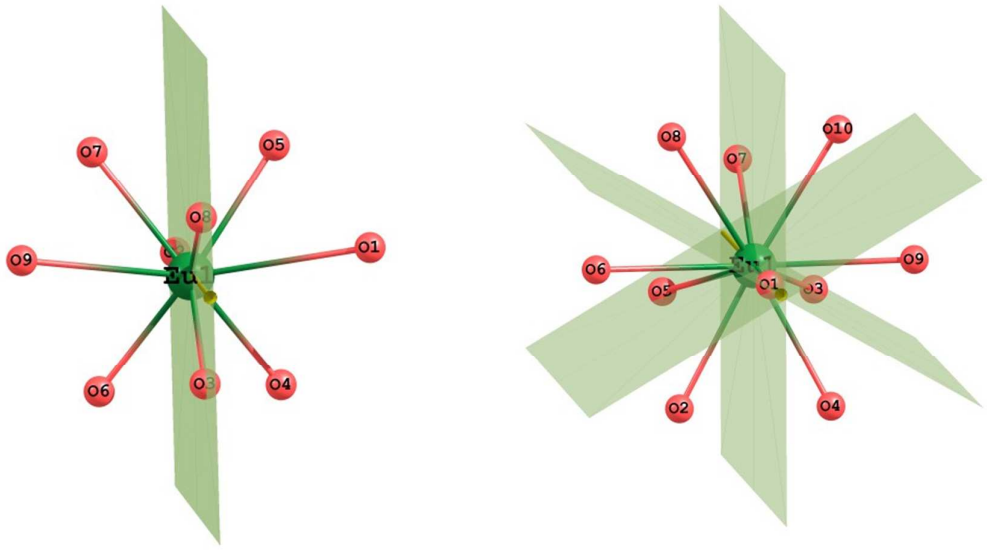

Figure 13: Nearest high-end symmetry observed for SrO_9 and SrO_{10}.

3.6. Conlusions:

In the present work, we have carried out an exhaustive experimental and theoretical investigation to get in depth knowledge about the local symmetry of SrO_9 and SrO_{10}polyheadra of Sr_2SiO_4.Undoped and lanthanide ion doped (Eu, Dy and Sm) doped Sr_2SiO_4 has been synthesized using sol-gel method. The same has been characterized using XRD and photoluminescence (PL) spectroscopy. Structurally it was found that there are two types of strontium polyhedra in strontium silicate asymmetric SrO_9 and relatively symmetric SrO_{10}. Local point group of these two polyhedra were determined using emission spectroscopy taking Europium as the probe ion which was further supported by theoretical measurements. Based on PL data and emission dynamics it was inferred that Eu occupy both 9- and 10-coordinated Sr in strontium silicate whereas Sm and Dy occupies specifically 9-coordnated Sr only. These results were further corroborated using Sr K-edge Extended X-Ray Absorption Fine Structure (EXAFS) measurement. Theoretical calculations using DFT also suggested that energetically Eu is stable at both the SrO_9 and SrO_{10}polyhedra whereas Sm and Dy destabilize the 10-coordinated Sr polyhedral by strenghting the individual metal oxygen bond.

Refernces:

1. J.Y. Park, J.Y.; Lim, M.A.; Kim, C.H.; Park, H.D.; Park, J. T.; Choi, S.Y. *Appl Phys. Lett.* **2003**, 82, 683-685

2. Lakshminarasimhan, N.; Varadaraju, U.V. *J. Electrochim. Soc*., **2005**, 152, H152-H156.
3. Sunitha, D.V.; Nagabhushana, H.; Sharma, S.C.; Nagabhushana, B.M.; Daruka Prasad, B.; Chakradhar, R.P.S. *Spectrochim. Acta. A*, **2014**, 127, 381-387
4. Nagabhushana, H.; Sunitha, D.V.; Sharma, S.C.; Daruka Prasad, B.; Nagabhushana, B.M., Chakradhar, R.P.S. *J. Alloys Compds.*, **2014**, 595, 192-199.
5. Song, Z. ; Ding, X. ; Yang, S.; Du., F.; Bian, L.; Duan, S.; Liu, Q.L. *J. Lumin*., **2014**, 152, 199-202.
6. Barzowska, J.; Chruścińska, A.; Przegietka, K.; Szczodrowski, K.; *Rad. Phys. Chem*., **2014**, 104, 31-35.
7. Tshabalala, M.A.; Swart, H.C.; Ntwaeaborwa, O.M.; *J. Vac. Sci. Tech. A*, **2014**, 32, 021401.
8. Xu, X.; Zhang, X.; Wang, T.; Qiu, J.; Yu, X. Mater. Lett. , **2014**, 127, 40-43.
9. Qin, J.; Lei, B.; Li, J.; Liu, Y.; Zhang, H.; Zheng, M.; Xiao, Y., Chao, K. *ECS J. Solid State Sci. Technol.*, **2013**, 2, R60-R64.
10. Catti, M.; Gazzoni, G.; Ivaldi, G., **1983**, 39, 29-34.
11. Gupta, S.K.; Pathak, N.; Thulasidas, S.K.; Natarajan, V.; *J. Lumin*, 2014, doi:10.1016/j.jlumin.**2014**.10.009
12. Gupta, S.K.; Bhide, M.K.; Kadam, R.M.; Natarajan, V.; Godbole, S.V. *J. Exp. Nanosci.,* **2015***,* 10, 610-621.
13. Gupta, S.K.; Mohapatra, M.; Kaity, S.; Natarajan, V.; Godbole, S.V. *J. Lumin*., **2012**,132, 1329-1338.
14. Gupta, S.K.; Kumar, M.; Natarajan, V.; Godbole, S.V. *Opt. Mater.,* **2013**, 35, 2320-2328.
15. Basu, S.; Patel, D.K., Nuwad, J., Jha, S. N.; Bhattacharyya, D.; Sudarsan, V.; Vatsa, R.K., Kulshreshtha, S.K. *Chem. Phys. Lett.* **2013**, 561–562**,** 82-86.
16. Basu, S.; Varma, S.; Shirsat, A.N.; Wani, B.N.; Bharadwaj, S. R.; Chakrabarti, A.; Jha, S. N.; Bhattacharyya, D. *J. Appl. Phys*., **2012**, 113, 043508.
17. Misra, N.L.; Yadav, A.K.; Dhara, S.; Phatak, R.; Mishra, S. K.; Poswal, A. K.; Jha, S. N.; Sinha A. K.; Bhattacharyya D. *Anal. Sci.* **2013**, 29, 579.
18. Yang , J.; Yang, L.; Liu, W.; Zhang, Y.; Fan, H.; Wang, Y.; Liu, H.; Lang, J.; Wang, *J. Alloys Compd.*, **2008**, 454, 506-509.
19. Nag, A.; Kutty, T.R.N. *J. Mater. Chem*. **2004**, 14, 1598-1604.
20. Chen, X.Y.; Liu, G.K. *J. Solid State Chem*. **2005**, 178**,** 419-428.
21. Chen, X.Y.; Zhao, W.; Cook, R.E.; Liu, G.K. *Phys. Rev. B*, **2004**, 70, 205122-1-205122-9.
22. Qiang, J.; Yongsheng, L.; Renfu, L.; Liu, L.; Wenqin, L., Xueyuan, C. *J. Phys. Chem. C* **2009,** 113*,* 2309-2315.
23. Konigsberger, D.C.; Prince, R. **1988,** Wiley, New York.
24. Newville, M.; Ravel, B.; Haskel, D.; Rehr, J.J.; Stern E.A.; Yacoby, Y. *Physica B*, **1995**, 208, 154-156.
25. Shannon, R. D. Acta Cryst. A, **1976**, 32, 751-767.
26. Nguyen, H.-D.; Yeo, I.-H.; Mho, S.-I. *ECS Transaction*, **2010**, 28, 167-173.
27. Haynes, W.M. CRC Handbook of Physics and Chemistry, 94th edition.